Efficient Pulsation Mitigation Modeling for Low Speed Open Jet Wind Tunnels with Helmholtz Resonator

Joseph C. Yen, Amir A. Kharazi, Edward G. Duell, and Joel Walter

Amentum Technology, Inc. (formerly Jacobs Technology, Inc.)
600 William Northern Blvd., Tullahoma, Tennessee, USA

Joseph.Yen@us.amentum.com
Amir.Kharazi@ us.amentum.com
Ed.Duell@us.amentum.com
Joel.Walter@us.amentum.com

Abstract: Recently the authors demonstrated a novel computational strategy for the simulation of the low frequency pressure pulsation phenomena that pertains to Göttingen style open jet wind tunnels (OJWT). The analysis strategy incurs very low computational cost and yet is predictive since the unsteady solution unequivocally reveals the airspeed dependence of the flow acoustics coupling physics. The work is now expanded to demonstrate the scope of mitigation control of the pressure pulsation using a Helmholtz resonator (HR) with the same OJWT geometry . The study begins with a simple benchmark acoustic problem to render a demonstration of the computational aeroacoustics (CAA) solver and an instructive review of a standing wave attenuation by HR on a looped straight waveguide. In the follow on wind tunnel study, the computer simulation reveals a strong effect by HR installation location on the effectiveness of pulsation attenuation. This effectiveness is demonstrated using a holistic presentation of the transient pressure response over the entire wind tunnel airline. The simulated antinodal HR installation is shown to significantly mitigate the pressure fluctuating amplitudes in the test section and along the rest of the airline duct. The current study renders an expanded understanding of the pressure pulsation phenomenon that is significant and valuable for continuous design improvement of OJWT. The tested computational strategy gives rise to a digital twin of an OJWT, particularly for pressure pulsation study. The computer model can provide accurate guidance and thus reduced costs for developing a subscale wind tunnel model experiment, which has been the most reliable but more expensive method for the development of pulsation mitigation design. With the predictive method of the OJWT digital twin, a significant reduction or eventual replacement of the laboratory effort in the future development of open jet wind tunnel airline may be possible.

1 Introduction

Helmholtz resonators (HR) have been used to mitigate the low frequency pressure pulsation phenomenon (Sellers et al., 1985) in Göttingen style low-speed open jet wind tunnels (OJWT). Several successful applications were reported (Waudby-Smith and

Contribution: 2025 FKFS Conference on Vehicle Aerodynamics and Thermal Management
15 – 16 October 2025 | Leinfelden-Echterdingen

Ramakrishnan, 2007; Duell et al., 2010; Kharazi et al., 2013; Best et al., 2023). The deployment design of HR usually depends on a subscale model of a wind tunnel under development. The experimental method is by far the most reliable and preferred approach, due to the lack of a predictive and computationally efficient tool for simulating the flow acoustics coupling phenomenon of pressure pulsation in a physical wind tunnel airline geometry.

Recently, an innovative computational strategy for the study of the pressure pulsation was proposed and demonstrated (Yen et al., 2025). The method was built on a non-conventional high resolution computational aeroacoustic (CAA) methodology and leveraged the low frequency nature of the physical problem in the computer model development. The computational strategy gave rise to a significant reduction in computational overheads while preserving the numerical resolution power for the unsteady flow field and companion acoustic field, both of which are necessary elements to the forming of the OJWT pressure pulsation phenomenon.

The previous study successfully revealed the conditional or staged intensification of the unsteady pressures when the airspeed was varied. In a most intensified pulsation condition, the same dominant frequency could be identified from both the preferred open jet vortex shedding mode and an excited longitudinal standing wave mode along the closed loop airline. This simulation result agrees very well with the long understood mechanism of the low frequency pressure pulsation phenomenon. In addition to showing frequency coincidence as explained by analytical methods (Arnette et al. 1999; Rennie, 2000), the computational method also predicts the fluctuating pressure amplitudes for quantitative assessments.

The same efficient, predictive computational strategy is expanded in this paper to the study of pulsation mitigation control with Helmholtz resonator (HR). Table 1 shows six cases that are included in the study whose solution will be discussed later in Section 4.1 through 4.6,

Table 1. Matrix of study

Case number	Computational model	Wind on/off
1	Baseline Closed-Return Open-Jet Wind Tunnel (OJWT)	On
2	Design Verification of 3.06 Hz Helmholtz Resonator	Off
3	Effect of HR on Acoustic Response with a Looped Long Straight Duct	Off
4	Installation of HR on Baseline OJWT at Pressure Node	On
5	Installation of HR on Baseline OJWT at Pressure Antinode #1	On
6	Installation of HR on Baseline OJWT at Pressure Antinode #2	On

respectively. The current study leverages the previous results to develop an HR of natural frequency that matches the dominant frequency in a most intensified pressure pulsation condition of the baseline OJWT (without HR). This HR design is then verified computationally using the same CAA solver with quiescent air. The effectiveness of the HR at attenuating a frequency matched standing wave is demonstrated next on a straight duct with the installation location at a pressure node and a pressure antinode, respectively. This case is a pure acoustic test condition with quiescent air, and the result provides a reference condition for comparison with the solution of the simulated OJWT airline with HR. The effect of the HR on the OJWT pressure pulsation is studied next with the resonator installed at each one of three locations that include one pressure node and two different pressure antinodes. These locations coincide spatially with the amplitude extremities of fluctuating pressure predicted by the baseline OJWT solution.

2 Open Jet Wind Tunnel Computer Model

Figure 1 shows a computer model of a modern design of Göttingen style automotive OJWT (Best et al., 2023). The wind tunnel is engineered for aeroacoustic testing purposes and includes several distinct noise control features. For example, the airline is shown to include elongated sound absorbing turning vanes in some corners and slanted wall design in the test chamber to prevent lateral standing waves. Aerodynamically the overall wind tunnel airline circuit is streamlined and generally produces a minimum overall pressure loss and therefore low power consumption. The overall centerline duct length of the full scale OJWT is about 224 m. This wind tunnel geometry is the basis of the baseline airline that was studied previously (Yen et al., 2025) for pulsation prediction demonstration. The same computer model will also be applied in the current study.

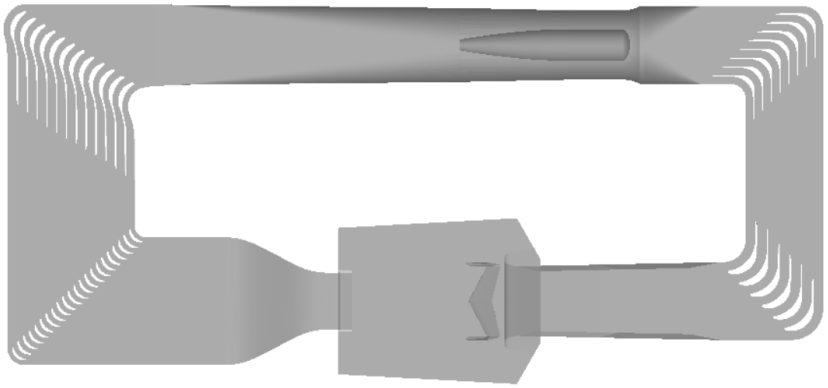

Figure 1. A modern closed return OJWT airline for aeroacoustic testing

Figure 2. Axisymmetric representation of open jet wind tunnel

It is computationally very costly to undertake a CAA simulation of the pressure pulsation phenomenon with the physical 3-D wind tunnel airline geometry. As reasoned in detail in the previous work, the low frequency nature of the problem permits the use of a simplified axisymmetric representation of the OJWT airline as shown in Fig. 2. As demonstrated previously with the same simplified airline geometry, the flow acoustic coupling physics was unequivocally revealed to predict the conditional intensification of the fluctuating pressures over a range of airspeed setpoints. In the axisymmetric geometry, the nozzle exit diameter (D) is 5.64 m based on which the airline length is about 40 D. The axial range of the open jet test section starts from the nozzle exit plane that is X/D=0 to the beginning of the collector at about X/D=2.5. More detail of the simulated test section geometry can be referred to the previous work.

The axisymmetric OJWT airline retains the effect of closed loop circuitry of the physical wind tunnel by imposing a paired cyclic boundary condition for the two far end boundaries of the linearized airline geometry. The computer model also mimics the actual wind tunnel by including an atmospheric vent in the test chamber, a fan model, and a heat exchanger model. These models are shown in Fig. 2. The vent is designed to provide an invariable pressure reference regardless of the airspeed. The overall energy balance of the closed airflow

system during a steady state running condition is sustained with the fan and heat exchanger models. More detail of the rationale and setup of these modelling features are detailed in the previous work (Yen, et al, 2025).

3 Computational Aeroacoustics Solver and Meshing Strategy

The computer simulation of the unsteady wind tunnel flow will be performed using an in-house developed JUSTUS code (Yen et al. 2010). The methodology of the solver is based on the method of space-time conservation element and solution element (abbreviated as CESE by the methodology originator Chang, 1995). It is an explicit method with a solution formulation that fundamentally complies with the hyperbolic nature of flow physics. The high resolution solution methodology also incorporates a time-accurate local time stepping scheme (Chang, 2003; Yen, 2011) whose implementation also complies with the non-conventional space-time flux conservation methodology of the CESE method. The local time stepping scheme facilitates a uniform numerical quality for the flow and acoustic solution across a space domain that is spanned by solution cells of very large size disparity for various resolution requirements. This solution capability feature is important for ensuring consistent solution quality anywhere in the wind tunnel air space. It is also very advantageous computationally because the solution method permits the use of very coarse cells for the air space outside the test chamber where the resolution of sound propagation is much more important and requires much lower mesh density than the bulk flow motion of small turbulence length scales. The solution method permits bespoke spatial resolutions in different locations that renders significant solution efficiency for the challenging flow acoustics coupling problem. The open jet solution is acquired using a method of implicit large eddy simulation (ILES) (Yen et al. 2010).

a)

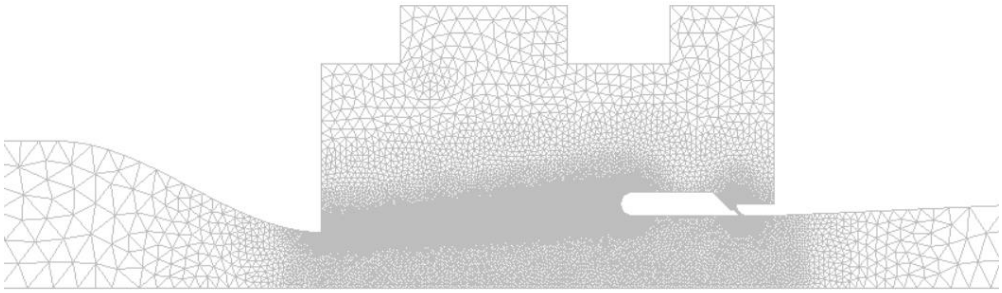

b)

Figure 3. a) Overall view and b) close-up view of unstructured triangular mesh

Figure 3 shows the computational mesh that was applied to study the baseline OJWT geometry (Yen, et al, 2025). The mesh includes all triangular cells with various levels of refinements where the finest mesh is designated for the open jet shear layer resolution and progressively coarser mesh is used elsewhere. As shown in Fig. 3, the coarsest mesh is present in the airline space outside the test chamber where the solution resolution requirement is set up to fully capture the passing sound waves that pertain to the pressure pulsation phenomenon. The coarse mesh also becomes a natural filter that damps off the flow and acoustic energy

that is associated with smaller length scales or wavelengths. The smaller mesh is also created near the proximity of HR connection to the airline duct. Figure 4 illustrates an example mesh refinement near the neck of HR. The detail of the mesh design can be referred to the previous work (Yen et al., 2025). The same meshing strategy for the axisymmetric wind tunnel geometry produces total cell count for different cases in the study ranging approximately from 52,000 to 57,000.

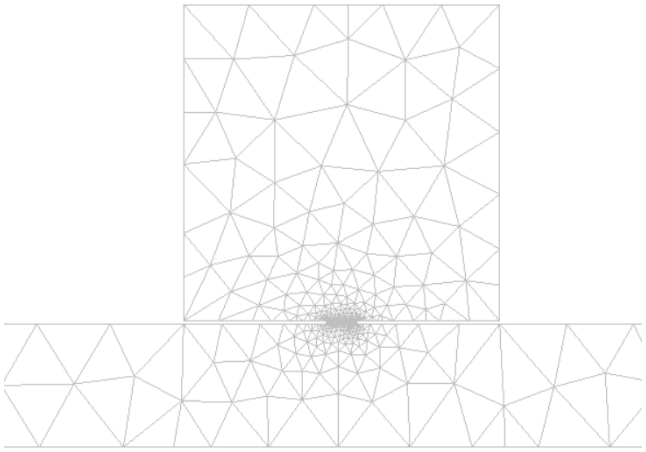

Figure 4. Example of mesh refinement near the neck of Helmholtz resonator on a duct

The previous work carefully examined the predicted time-averaged flow properties and statistical result of the turbulent open jet solution by comparing to applicable theories. Very good agreement was found, which verified the solution capability of the computational solver and meshing strategy. The current study applies the same computational strategy for the different demonstration cases of pulsation mitigation study using Helmholtz resonator. To provide a consistent quality of unsteady solution with the previous work, the same Courant–Friedrichs–Lewy (CFL) number of 0.75 is used here for the solution time integration. The minimum solution time step size for the different cases in the study ranges from approximately 1.2e-5 s and 1.5e-5 s based on the chosen CFL value and the design of the unstructured triangular mesh. The minimum time step size pertains to the smallest cell sizes and larger cells will naturally incur larger time step sizes during the solution time marching process, as defined in the applied local time stepping method (Yen, 2011).

The 2D axisymmetric wind tunnel model neglects several loss factors in the real wind tunnel such as wall boundary layers, flow conditioning and cornering devices, high loss elements in the heat exchanger. This condition represents a reduced damping factor to counter the intensification of flow acoustics coupling. That is to say that the simulated resonance condition is expectedly to produce pressure perturbation amplitudes that are higher than the real wind tunnel data. In addition, the 2D problem setting is also a compounding factor for higher perturbation amplitude prediction, due to the more coherent shedding vortices than in 3D and therefore a stronger forcing function to produce a more intensified result of pressure pulsations. Despite the expected higher amplitude prediction, the proposed solution strategy remains useful of providing efficient assessment of relative effects on pulsation tones and amplitudes for the study of changes in geometry and boundary conditions.

4 Results and Discussion

The airspeed setpoint in each case of the study is determined by the velocity solution inside the nozzle of the simulated wind tunnel airline. In a calculation, the setpoint is reached by

varying the pressure rise of the fan model (to replenish the momentum of the wind tunnel flow) until the transient solution reveals a stable oscillatory response about the target airspeed. The temperature setpoint at the same nozzle location is reached with removal of the increased flow internal energy by the heat exchanger model (to remove the dissipated heat from the turbulent open jet flow). The fan pressure rise cannot be known accurately a priori and therefore the arrival of an airspeed setpoint requires an iterative calculation process until the target airspeed is reached.

The previous work (Yen et al., 2025) showed that both the airspeed and temperature setpoints could be reached and became sustaining after the wind tunnel flow solution was developed for 60 s or about 180 cycles of the most intensified frequency of the flow perturbation. To report the transient solution after the initial 60 s of run time, the stable fluctuating solution is further developed for another 12 s or about 36 cycles to provide a sufficient population of transient data points. This extended solution time is important for statistical quality due to the nonstationary nature of turbulent wind tunnel flow. The nonstationary flow nature is commonly experienced in a real-world wind tunnel condition. The required two-stage solution development would be very costly computationally if a 3-D wind tunnel model were to be applied to tackle the problem. In contrast, the computational strategy proposed in the current study is quite affordable as an efficient design tool due to the capability of rendering a quick solution turnaround time.

The study examines the perturbation pressure based on root-mean-square (RMS) values to assess the magnitude of the pulsation phenomenon. The companion turbulent kinetic energy (TKE) inside the open jet shear layer will also be examined. The holistic map of the perturbation pressures will be presented. The perturbation pressure is calculated by subtracting the time-averaged pressure from the predicted pressure solution at each solution location of the entire wind tunnel domain. The TKE as presented is calculated based on the perturbation velocity by subtracting the time-averaged velocity from the predicted transient velocity solution. The reported perturbation pressures and TKE are nondimensionalized based on the dynamic pressure and kinetic energy at the setpoint airspeed value.

4.1 Baseline Closed-Return Open-Jet Wind Tunnel (OJWT)

The baseline condition was previously investigated using the same computational strategy reported in the current study. The predicted result showed a most intensified condition of pressure pulsation whose oscillating energy peaked sharply at 3.08 Hz frequency with a 50 m/s airspeed setpoint. This frequency coincides with the 3.06 Hz which is the fourth longitudinal eigenmode (Kinsler, et al, 1982) of the simulated wind tunnel airline. This baseline solution is a reference condition that does not include any pulsation mitigation applied to the simulated wind tunnel geometry. The baseline geometry applies a neutral horizontal position of the collector flap in the test section and the pressure shell effect of the airline duct is intact without inadvertent venting (such as air leaks through the perimeter of an access door). For comparison to the baseline solution, the simulation of the current study for mitigation control demonstration is performed at the same 50 m/s airspeed setpoint.

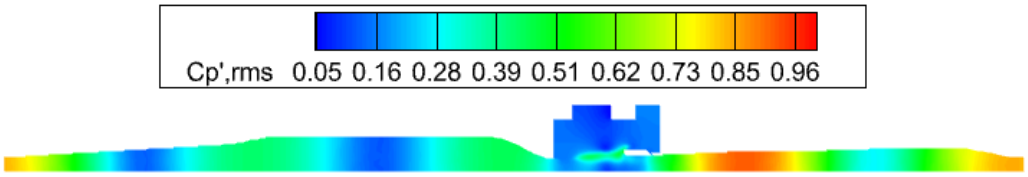

Figure 5. Perturbation pressures of baseline condition of open jet wind tunnel

Figure 5 shows the previously predicted solution whose perturbation pressures are now analyzed to present the root-mean-square (RMS) values. The $C_{p',rms}$ is calculated using the transient pressure solution collected after a steady response solution is reached. The statistical calculation is made where the pressure perturbations (in reference to the time averaged value) are nondimensionalized by the flow dynamic pressure at the airspeed setpoint. Figure 5 highlights important observation also reported previously (Yen et al., 2025). The pressure solution shows a clear pattern of standing wave along the simulated airline where repeated crests and troughs of perturbation pressure can be identified. The axial spacings between consecutive amplitude peaks are approximately 10 D in reference to the nozzle diameter (D) of the linearized axisymmetric airline. The predicted peak pressure amplitudes are higher in the airline duct downstream of the test section in comparison to the upstream.

The baseline pulsation result obtained from the previous work will be included for comparison in the following discussion. The predicted peak pulsation frequency will also be the basis for the Helmholtz resonator design to be used in the demonstration of pulsation mitigation simulation based on the advocated computational strategy.

4.2 Design Verification of 3.06 Hz Helmholtz Resonator (HR)

The use of Helmholtz resonator (HR) for pulsation attenuation is inspired by the postulated theory that the coupling between the unsteady open jet vortex shedding modes and frequency-matched longitudinal acoustic eigenmodes along the wind tunnel airline would give rise to more pronounced amplitudes of the unsteady pressures when compared to a neutral nonstimulated open jet condition. A successful working of HR is thought to weaken or break the coupling mechanism between the forcing function by the flow induced perturbation and the responses of the acoustic airline eigenmode. Based on this premise and the baseline solution, a 3.06 Hz Helmholtz resonator is developed and computationally verified. The verification simulation is made with the HR on a simple straight waveguide whose cross sectional area is four times the neck opening area of the resonator. The acoustic solution is acquired using the full (instead of linearized) Euler solver of the JUSTUS code.

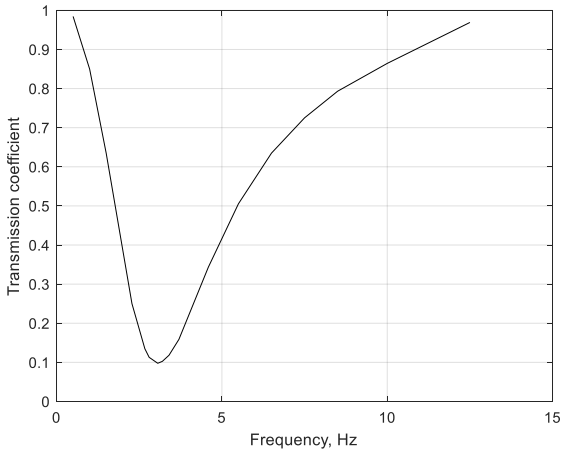

Figure 6. Predicted transmission curve of a 3.06 Hz Helmholtz resonator

Figure 6 shows the predicted transmission coefficient curve of the HR over a range of forcing frequencies. As shown, the result resembles the response of a bandpass filter (Kinsler et al., 1982) in which the design frequency is centered at 3.06 Hz where a transmission coefficient of 9.8% is shown in reference to the simulated sound source power. This 3.06 Hz Helmholtz resonator geometry will be applied thoughout this pulsation mitigation study

In this verification study, the HR is predicted to block and reject 90.2% of the incoming sound power back toward the source end. The 9.8% remaining sound power would pass over the HR location toward the opposite end of the sound source. The rejected sound wave and transmitted sound wave do not get to interact in the simulated condition with the open ended ductwork. When the ductwork becomes looped as in a closed return wind tunnel airline, such a wave interaction would occur and produce some form of standing wave. This condition will be studied next.

4.3 Effect of HR on Acoustic Response with a Looped Long Straight Duct

The acoustic attenuation effectiveness of the 3.06 Hz HR is first examined in a simple problem setting with a standing wave along a looped long duct with quiescent air. The looping of the long duct at the two far end boundaries is simulated based on a paired cyclic boundary condition as also applied in the baseline closed return OJWT model (Yen et al., 2025). Figure 7 shows the computer model of the long duct with HR installed separately at the pressure node and antinode. The location of the sound source is shown by a darkened line segment between two circular markers denoting the range of the sound source. The duct length is chosen to be the same as the 40 D long OJWT airline, which equals to two wavelengths of a 3.06 Hz sound wave at 20° C. The acoustic sound source is located on the duct wall over the axial range that coincides with the range of the flow collector in the simulated OJWT test section. The radius of the duct is set to equal to the axial range of the sound source such that the sound emitting surface area of the source equals to twice the duct cross sectional area. The sound source is assumed to emit a coherent pressure at 1.0 Pa peak amplitude ($\frac{1}{\sqrt{2}}$ Pa RMS), and the problem setting would produce a left running and a right running sound waves along the duct of the same 1.0 Pa peak amplitude ($\frac{1}{\sqrt{2}}$ Pa RMS). In an uncontrolled condition, a standing wave is expected to form with 2.0 Pa peak amplitude ($\sqrt{2}$ Pa RMS). This subset problem of the current study includes a baseline case and two controlled cases with the HR at a pressure node and at a pressure antinode, respectively. The locations of node and antinode are determined from the baseline standing wave solution. The problem setting would produce multiple nodes and antinodes, and without losing generality for attenuation discussion only those to the right hand side of the sound source are included in the acoustic study.

a) HR installed at a pressure node

b) HR installed at a pressure antinode

Figure 7. Installation of Helmholtz resonator on a long duct

Figure 8 shows the predicted root-mean-square (RMS) pressure contour map of the acoustic response of the three cases in the study. Figure 9 displays the same pressure response result as a function of axial displacement from a X=0 location. The X=0 reference location coincides with the nozzle exit of the OJWT, whose longitudinal length is 40 D. The baseline result shown in Fig. 8a reveals a clear pattern of standing wave where it shows equally spaced, alternate minimum and maximum amplitudes along the long duct. As detailed in Fig. 9, the peak RMS value is about 1.4 Pa and the peak-to-peak spacing is 10 D. This predicted standing waveform result agrees with the theory result, as discussed previously. Figure 8b shows the solution with the HR at the first pressure node to the right of the sound source. As shown in Fig. 9, the predicted standing wave pattern is nearly unchanged except for a slightly higher

peak amplitude than the baseline. Figure 8c shows the result with the HR installed at the first pressure antinode to the right hand side of the sound source. Compared to the other two cases, the result of the HR at the antinode shows a weakened standing waveform of lower peak amplitude. The original antinode location of the HR installation is turned into a node and the phase of the standing waveform is shifted by 5 D distance (one half of the 10 D peak-to-peak

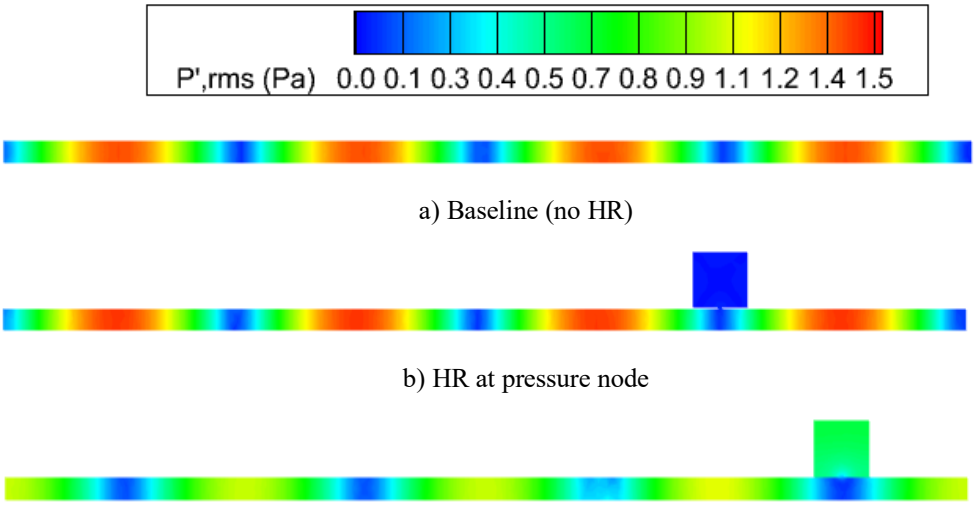

a) Baseline (no HR)

b) HR at pressure node

c) HR at pressure antinode

Figure 8. Acoustic pressure in root-mean-square values

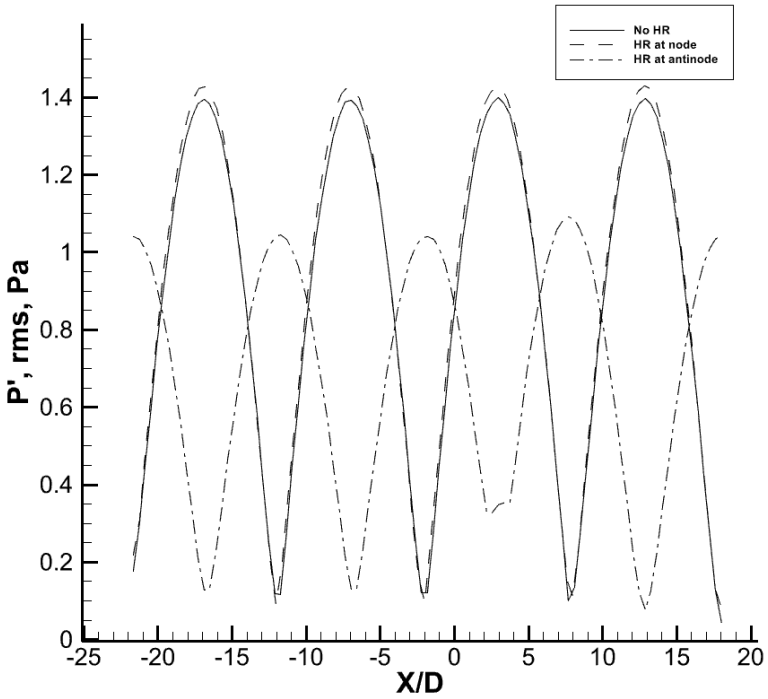

Figure 9. Variation of acoustic pressure along duct

spacing). The peak RMS amplitude is seen to reduce to about 1.05 Pa, which is 25% lower than the baseline condition.

The result of the antinode HR installation in Fig. 9 also represents a reduced standing wave ratio (SWR) (the ratio of the antinode to node amplitude) when compared to the baseline condition. This suggests the modified standing wave is now comprised of two opposite traveling waves of different amplitudes. This amplitude disparity may be understood from the result of the HR design verification in Fig. 6. The HR produces a reduced transmitted sound energy and therefore a lowered sound pressure. In the simulated standing wave condition, the reduced sound amplitude wave, after being looped to the other duct end, becomes a right running wave to interact with the left running wave of unattenuated sound pressure from the sound source. The wave interacting result would not be a strict standing wave but includes some left running wave component due to the higher amplitude of the constituent left running sound wave from the source. The amplitude disparity also gives rise to lower resultant wave amplitude in comparison to the unattenuated condition.

This simple problem demonstrates that when installed at a pressure node the Helmholtz resonator (HR) is not effective of attenuating the standing wave in the looped waveguide. In contrast, the attenuation becomes significant when the HR is at a pressure antinode. In the baseline wind tunnel geometry, there is no efficient energy dissipating mechanism for infrasound (lower than 20 Hz). The working of HR does not produce energy dissipation of the infrasound power. Instead, the capability of weakening a standing wave is hypothesized to come from mitigating the acoustic feedback excitation due to airline longitudinal eigenmodes that escalates the open jet unsteadiness.This would further fuel the standing wave energy into the otherwise uncontrolled increase of very intensified pressure pulsation in the flow acoustic coupling phenomenon. In this sense, the role of the HR is attributed to decoupling the infrasound excitation from the open jet unsteadiness.

4.4 Installation of HR on OJWT at Pressure Node

The effect of Helmholtz resonator on pulsation attenuation is first studied with the 3.06 Hz HR installed at X=11.8 D, which is the first pressure node in the downstream of the collector based on the baseline wind tunnel solution in Fig. 5. Figure 10 shows the predicted perturbation pressure solution over the entire wind tunnel airline. The holistic response map also reveals a clear pattern of standing waveform that is very similar to that of the baseline result in Fig. 5 except that the peak pressure amplitudes are reduced slightly. The nodal HR installation location remains essentially as a pressure node, where the response amplitude is a minimum locally.

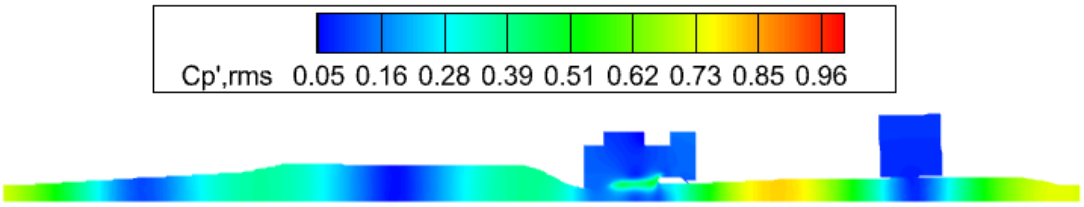

Figure 10. Perturbation pressures of open jet wind tunnel with HR at pressure node

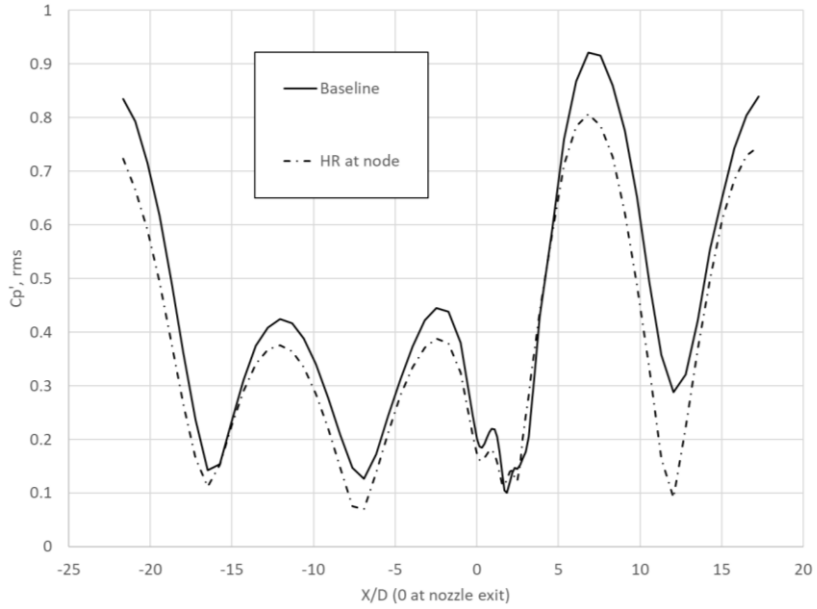

Figure 11. Perturbation pressures along airline

Figure 11 shows a comparison of perturbation pressures along the centerline of the linearized airline. As shown, the standing waveform retains the same amplitude peak-to-peak spacing while the nodal HR produces about 13% of peak amplitude reduction from the baseline condition. The result of no phase shift in the standing waveform is similar to that in the Figs 8b and 9 for the nodal HR on a straight duct. In that quiescent flow acoustic study (Sec. 4.3), the simulated sound source strength is kept unchanged. In the wind-on OJWT, the source of pressure perturbation is the flow unsteadiness of the test section open jet, which is susceptible for acoustic excitations, particularly the low frequency longitudinal eigenmodes of the wind tunnel circuit. Despite that the nodal HR is not expected to significantly alter the acoustic response to the source of perturbation, the predicted 13% reduction in the peak response pressure reiterates the acoustic susceptibility of the open jet unsteadiness and suggests a design that acoustically decouples the open jet perturbation and longitudinal circuit modes to be a potentially effective means to mitigate the pressure pulsation problem.

Figure 12 shows the companion frequency spectrum of the open jet turbulent kinetic energy (TKE) with comparison to the baseline solution. As shown, the overall shape of the TKE spectrum remains largely unchanged. The prediction shows compliance to the postulated -5/3 slope energy cascading law in frequency range that are higher than the interested low frequencies of pressure pulsations. The TKE reveals a steeper decay for frequencies higher than 50 Hz. This result shows a proof of sufficient spatial resolution of the applied numerical method for the transient open jet flow. As also shown in Fig. 12, the primary peak energy of the vortex shedding frequency stays sharply at about 3.06 Hz as seen in the baseline condition. The HR gives rise to a slight reduction in the peak energy of the flow unsteadiness and also some different secondary peaks. From the standpoint of unsteady flow energy over the entire frequency spectrum however, the effect of the nodal HR is insignificant to incur changes to the open jet flow unsteadiness.

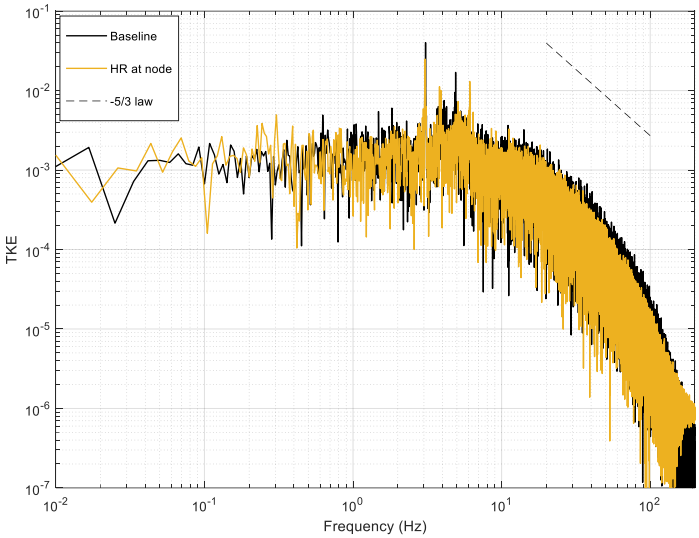

Figure 12. Frequency spectrum of turbulent kinetic energy (TKE) inside open jet shear layer

The turbulence property reported in Fig. 12 is surveyed inside the open jet shear layer that is located at X=1.75 D and on the nozzle lip line (0.5 D radial distance from centerline). In the baseline wind tunnel solution (Yen et al., 2025), this axial location revealed self-similar shear layer velocity profile where the TKE cascading in the frequency spectrum showed a decaying trend that complied with the -5/3 slope law as postulated to take place in the inertial subrange (Tennekes and Lumley, 1972; Wilcox, 1998). The same location will be used for the TKE reporting throughout the study.

4.5 Installation of HR on OJWT at Pressure Antinode #1

The baseline OJWT solution shows the first pressure antinode downstream of the test section is located at X=7.7 D. This is the first antinode location chosen to demonstrate the effectiveness of the 3.06 Hz HR for pulsation attenuation. Figure 13 shows the predicted perturbation pressures. In a stark difference from the strong pulsation condition in Figs. 5 and 10, the amplitudes of the perturbation pressure are significantly diminished along the entire airline. The strong standing waveform in the baseline wind tunnel and the nodal HR installation case no longer prevails. As presented in Fig. 13, the perturbation pressure amplitudes become so low that the only region of appreciable fluctuations is inside the open

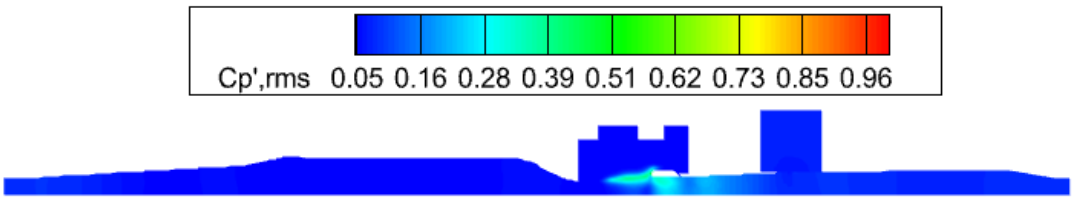

Figure 13. Perturbation pressures of open jet wind tunnel with HR at pressure antinode #1

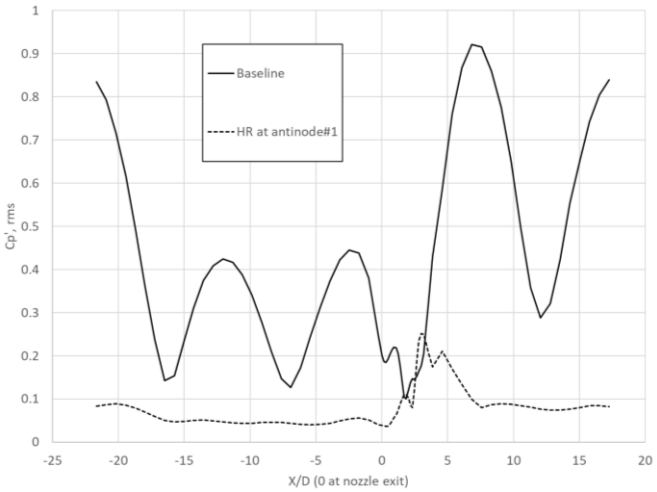

Figure 14. Perturbation pressures along airline

jet shear layer and the downstream airline duct until the resonator location. The perturbation amplitudes inside the shear layer are also reduced in comparison to the two much intensified conditions in Figs. 5 and 10.

Figure 14 shows the centerline Cp', rms as a function of the axial displacement from the nozzle exit. The result clearly echoes the result in Fig. 13 regarding the highly effective pulsation attenuation result with HR at the first antinode location. Outside the test chamber, the perturbation pressure along the airline is reduced to below 10% of the nozzle exit dynamic pressure. In contrast, the Cp', rms is higher than 92% with the baseline wind tunnel airline. The waveform of the pressure perturbations reveals a quicker variation (smaller wavelength) in a small axial range between X/D=0 and 5.0. This is related to the hydrodynamic signature imposed by the open jet vortex shedding. The attenuation effect of the HR can be seen in the test section range (bewteen X/D=0 and 2.0) to produce 5 to 6 times reduction from the peak perturbation pressure of the baseline condition.

Figure 15 shows the frequency spectrum of the TKE inside the open jet shear layer. The sharp peak of the turbulence energy at 3.06 Hz in the baseline condition is eliminated with the HR at the first antinode (denoted as AN#1 in Fig. 15). The controlled condition generates a few secondary frequency peaks and the overall broadband spectrum of the TKE resembles the baseline result except for slightly lower energy above 30 Hz. The computed turbulence solution retains the compliance with the -5/3 law of energy cascading rate in a frequency range that are higher than the interested perturbation infrasound. Steeper turbulence energy decay occurs at frequencies higher than 30 Hz.

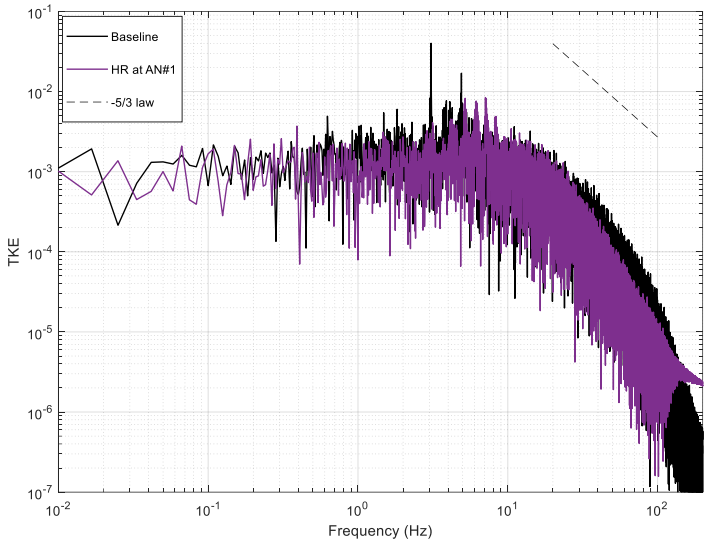

Figure 15. Frequency spectrum of turbulent kinetic energy (TKE) inside open jet shear layer

4.6 Installation of HR on OJWT at Pressure Antinode #2

The second pressure antinode in the test section downstream is located at about 15.7 D distance from the nozzle exit. The 3.06 Hz HR installed at this location is studied next. Figure 16 shows the contour map of the predicted perturbation pressure over the entire wind tunnel airline. Similar to the result of HR at the first antinode, the effect of pulsation attenuation is also significant. The standing wave in the baseline airline condition is largely diminished and the appreciable fluctuations are now only seen between the collector and the HR installation location. The magnitude of perturbation pressures inside the open jet shear layer remains high as was the case with the HR at the first antinode but much weaker in comparison to the baseline condition with more intensified pulsations.

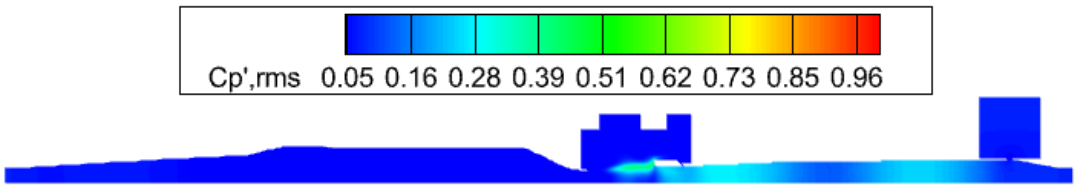

Figure 16. Perturbation pressures of open jet wind tunnel with HR at pressure antinode #2

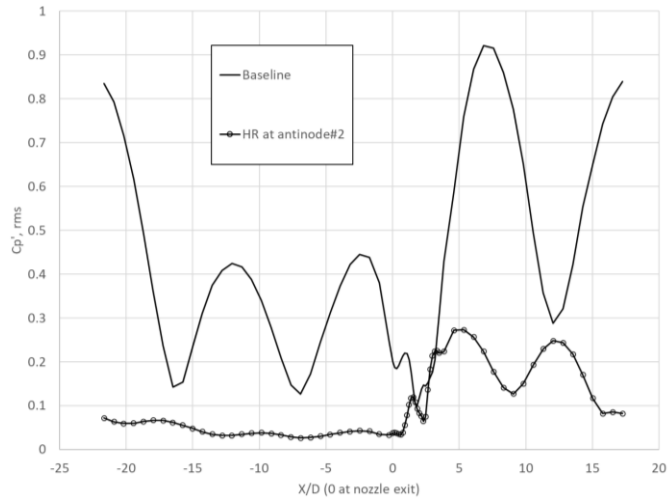

Figure 17. Perturbation pressures along airline

Figure 17 shows the Cp', rms distribution over the airline. The result confirms the effective pulsation attenuation result shown in Fig. 16. The amplitudes of the perturbation pressure remain below 10% of the nozzle dynamic pressure in the airline upstream of test section. In the downstream, a stronger standing wave pattern can be seen with 27.3% maximum peak amplitude until the second pressure antinode. Attenuation on the test section pulsation level is also quite similar to the result of the HR at the first antinode. Although not as visible in Figs.13 and 14, the HR at the second antinode in Figs. 16 and 17 produces a weakened standing wave remnant that is confined to the axial range between the test section and the HR location. The peak-to-peak distance of the standing wave also becomes shorter than that in the baseline wind tunnel condition. This suggests that the most intensified response frequency has been modified to a higher frequency.

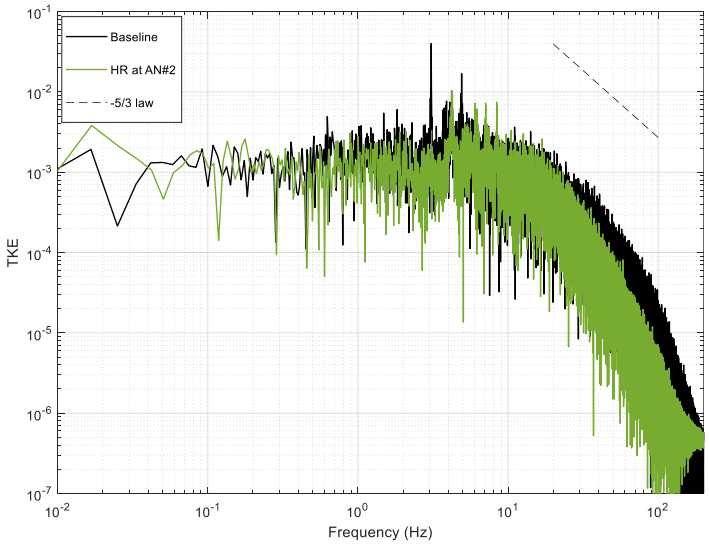

Figure 18. Frequency spectrum of turbulent kinetic energy (TKE) inside open jet shear layer

Figure 18 shows the frequency spectrum of the TKE inside the open jet shear layer for this antinal HR case (denoted as AN#2 in Fig.18). Figure 18 shows a very similar result to Fig.

15 that includes the elimination of the most dominant peak frequency, generation of secondary peaks and slightly lower turbulence energy in the broadband frequency range above 30 Hz. The predicted turbulence energy cascading again shows compliance with the -5/3 slope law over the frequency range between 10 Hz and 30 Hz, followed by a steeper decay rate in the higher frequencies.

5 Conclusion

An innovative and very efficient predictive computational strategy was successfully demonstrated in a previous study that pertained to the prediction of low frequency pressure pulsation phenomenon in a Göttingen style open jet wind tunnel. This study applied the same computational strategy and extended the work to demonstrate the predictive solution capability on pulsation mitigation using Helmholtz resonator (HR). It is anticipated that the new computational technique can supplement or eventually replace physical experiments at model scale whose objective is to identify and eliminate problematic pulsation in new full scale wind tunnel design. The demonstration again proved the computational efficiency and accurate nature of the computational aeroacoustic solver JUSTUS together with the applied analysis strategy. The computer simulation presented a holistic picture of the pressure pulsation over the entire wind tunnel airline. This solution capability provides detail of the formation of standing waves along the airline in different controlled scenarios with the HR. The study clearly demonstrated a strong dependence of pulsation attenuation on the HR installation location.

6 Reference list

Arnette, S., Buchanan, T., and Zabat, M., "On Low-Frequency Pressure Pulsations and Static Pressure Distribution in Open Jet Automotive Wind Tunnels," SAE Technical Paper 1999-01-0813, 1999

Best, S., Bari, G., Brooker, T., Flynt, G., Walter, J., and Duell, E., "The Honda Automotive Laboratories of Ohio Wind Tunnel," SAE Int. J. Adv. & Curr. Prac. in Mobility 5(6):2116-2137, 2023.

Chang, S. C., "The Method of Solution-Time Conservation Element and Solution Element – A New Approach for Solving the Navier-Stokes and Euler Equations," Journal of Computational physics, 119, 295-324, 1995.

Duell, E. G., Kharazi, A. A., and Muller, S., Ebeling, W., and Mercker, E. "The BMW AVZ Wind Tunnel Center," SAE Paper No. 2010-01-0118.

Kharazi, A., Duell, E., Walter, J. Application of Helmholtz Resonators in Open Jet Wind Tunnels. SAE Int. J. Passeng. Cars-Mech. Syst. 2013, 6, 436–447.

Kinsler, L. E. Frey, A. R., Coppens, A. B., and Sanders, J. V., "Fundamentals of Acoustics," 3rd ed., 1982, John Wiley and Sons.

Rennie, M., "Effect of Jet Length on Pressure Fluctuations in ¾-Open Jets", Motor Industry Research Association Vehicle Aerodynamics 2000 Symposium, October 2000.

Sellers, W.L.I.; Applin, Z.T.; Molloy, J.K. "Effect of Jet Exit Vanes on Flow Pulsations in an Open-Jet Wind Tunnel," Technical Report NASA-TM-86299; Langley Research Center: Hampton, VA, USA, 1985.

Tennekes, H. and Lumley, J. L., "A First Course in Turbulence," by The MIT Press, 1972.

Waudby-Smith, P. and Ramakrishnan, R., "Wind Tunnel Resonances and Helmholtz Resonators," Canadian Acoustics/Acoustique Canadienne, Nov. 35, No.1, 2007

Wilcox, D. C., "Turbulence Modeling for CFD," 2nd ed., by DCW Industries Inc., 1998.

Yen, J. C., Kimbrell, A. B., and Connor, C. H. "Study of WICS Data Using an Emerging Lower-Order CAA Method," AIAA 2010-1742

Yen, J. C., "Demonstration of a Multi-Dimensional Time-Accurate Local Time Stepping CESE Method," AIAA-2011-2755.

Yen, J., Duell, E., Walter, J., Kharazi, A., “CAA Study of Helmholtz Resonator Application on Edge-Tone Noise Suppression”, AIAA-2012-2103.
Yen, J. C., Duell, E. G., Muller, S. A., “An Acoustic Resonance Study with an Open-Jet Wind Tunnel Geometry Using a Time-Accurate Local-Time-Stepping CESE Method,” AIAA 2019-2626.
Yen, J. C., Kharazi, A. A., Duell, E. G., Walter, J., “An Efficient CAA Strategy for Studying Flow-Acoustics Coupling Phenomenon in Low-Speed Closed-Return Open-Jet Wind Tunnels,” AIAA 2025-3689.